


Vibration suppression of wind turbine nacelle with active electromagnetic mass damper systems using adaptive backstepping control

Sinan Basaran¹ , Fevzi Cakmak Bolat² and Selim Sivrioglu³

Journal of Vibration and Control
2021, Vol. 0(0) 1–14
© The Author(s) 2021
Article reuse guidelines:
sagepub.com/journals-permissions
DOI: 10.1177/1077546321998878
journals.sagepub.com/home/jvc


Abstract

Many structural systems, such as wind turbines, are exposed to high levels of stress during operation. This is mainly because of the flow-induced vibrations caused by the wind load encountered in every tall structure. Preventing the flow-induced vibration has been an important research area. In this study, an active electromagnetic mass damper system was used to eliminate the vibrations. The position of the stabilizer mass in the active electromagnetic mass damper system was determined according to the displacement information read on the system without using any spring element, unlike any conventional system. The proposed system in this study has a structure that can be implemented as a vibration suppressor in many intelligent structural systems. Two opposing electromagnets were used to determine the instant displacement of the stabilizer mass. The control currents to be given to these electromagnets are determined by using an adaptive backstepping control design. The adaptive controller algorithm can predict the wind load used in the controller design without prior knowledge of the actual wind load. It was observed that the designed active electromagnetic mass damper structure is successful in suppressing system vibrations. As a result, the proposed active electromagnetic mass damper system has been shown to be suitable for structural systems in flow-induced vibration damping.

Keywords

Vibration suspension, electromagnetic actuator, wind turbine, backstepping control

1. Introduction

Suppressing the structural or mechanical vibration has significant applications in engineering systems. Nowadays, many structural systems are designed to cope with the vibrations to be exposed during the design phase. In vibration suspension operation, active (Alkhatib and Golnaraghi, 2003; Zhao et al., 2020), passive (Soong and Constantinou, 2014), and semi-active methods can be used (Bathaei et al., 2018; Hiramoto and Grigoriadis, 2016). The most fundamental form of vibration suppression systems is an added external mass that suppresses the vibration of the system with spring and damper elements. In the literature, this system is referred to as tuned mass dampers (TMDs) (Elias et al., 2019; Lackner and Rotea, 2010; Kwok and Samali, 1995; Martynowicz, 2019; Miyata, 2003; Tian et al., 2019). The value of the spring and damper elements in these systems is constant and determined by preliminary design work. Li and Cui (2017) investigated the nonlinear behavior of the spring element in a TMD system and gave a comparison with the linear TMD system. Among the structural systems, wind turbines are the most common systems in

which flow-induced vibration prevention is important. Martynowicz (2017) studied wind turbine tower nacelle with a magnetorheological TMD system with numerical modeling and experimental analyses to deal with the dynamic load of the system. In addition, he then reported application of different control strategies on the semi-active MR damper element in the test rig of a wind turbine tower nacelle system by applying different vibration loads including aerodynamic loads (Martynowicz, 2016).

¹Department of Mechanical Engineering, Bilecik Seyh Edebali University, Bilecik, Turkey

²Department of Mechanical Engineering, Bolu Abant İzzet Baysal University, Bolu, Turkey

³Department of Mechanical Engineering, Antalya Bilim University, Antalya, Turkey

Corresponding author:

Sinan Basaran, Department of Mechanical Engineering, Bilecik Seyh Edebali University, Gulumbe Campus, Merkez/Bilecik 11230, Turkey, Turkey.
Email: sinan.basaran@bilecik.edu.tr

On the other hand, it is reasonable to use passive vibration isolators in situations where the system internal damping is high, but passive methods are inadequate for completely suppressing vibrations. Active methods in vibration suspensions are more reliable because of the adaptation features for the changes in disturbance load conditions. In the active methods, to prevent vibration of the structural system, the controller with a closed-loop system is used to generate controller force with actuators. In literature, it is possible to see many structures designed with different active control strategies and different actuators (e.g., Coppola and Liu, 2010; Contreras-Lopez et al., 2019; Coppola et al., 2013; Talib et al., 2019). Fitzgerald and Basu (2013) developed an active structural control scheme to control wind turbine nacelle tower vibration. They designed an active tuned mass damper (ATMD) which is placed inside the turbine nacelle. Another area where an ATMD structure is applied is the offshore wind turbines. Brodersen et al. (2016) worked on eliminating the vibrations of a tower under wind load with the actuator added on the nacelle. Huo et al. (2007) proposed a design of a linear H_∞ control of an active mass damper (AMD) for vibration reduction of the buildings. In their study, they proposed a controller and standard mass damper actuator that can work in the uncertainties of mass and stiffness values. Ikeda (2016) in his work proposed a method that uses the results of system identification in the field of active structural control and gave the numerical example of the linear quadratic regulator control of the building structure with the AMD. Hacıoglu and Yagiz (2011) presented the Lyapunov-based backstepping controller with a simulation model applied to a nine-story building model with a TMD installed on the top floor. They used real earthquake data as an excitation to the building model. A comparison of the performance for active and passive vibration suppression systems was done by Ricciardelli et al. (2003). In their works, they showed the performance comparison between TMD, AMD, and ATMD systems and gave simulated results in the frequency domain.

To increase the efficiency of the active vibration suppression systems, we propose an electromagnetic actuator in this study. In a conventional TMD system, there is no actuator to provide any movement for the external mass (Arrigan et al., 2010; Sladek and Klingner, 1983; Sun and Jahangiri, 2018; Wu et al., 2018). In the AMD system, the mass is moved by the actuator with a closed-loop control.

In this study, we propose an electromagnetic actuator to move the mass of the damper. Two opposite electromagnetic actuators are used to move the external or active mass. The proposed new structure is called active electromagnetic mass damper (AEMD). A feedback control structure is necessary for the proposed AEMD system to suppress the vibration of a wind turbine. When the control current passes over the coil in the electromagnets, a magnetic force is

generated, and this magnetic force moves the external ferromagnetic mass to suppress the vibration of the main structure. In the AEMD design, the selection of the stabilizer external mass was parameterized, and four different cases were investigated in this study.

Adaptive control is a technique used to control various systems whose parameters are unknown, indeterminate, or changing (Sivrioglu, 2006). In the proposed AEMD system, we implement the adaptive backstepping algorithm. The wind load acts as the driving force for vibration, so it is necessary to know its value during the control operation of the system. However, it is not always possible to measure the wind load. The controller designed in this study will also be adapted to the wind load which is thought to be time-varying but unknown. Two different assumptions were made for wind load, and simulation studies were conducted. First, the model has assumed the wind load is constant and acts in a certain period of time. Then, simulation studies were carried out with the variable wind load model.

This article is organized as follows: In Section 2, we present the AEMD system. The mathematical model of the system is given in the next section. In Section 4, a Lyapunov-based adaptive backstepping control design is given. Simulation studies and results are given in the following sections, respectively. Finally, the verification of the electromagnetic control force results with the electromagnetic finite element analysis method given in Section 6.

Notations: In this article, \mathbb{R} denotes the set of real numbers, superscript \mathbb{R}^n denotes the n -dimensional space, boldface capital letters represent the matrices, the transpose of the matrix A is denoted by A^T , and the first and second derivatives are denoted by superscripts “.” and “..” respectively.

2. Active electromagnetic mass damper systems

The schematic view of the wind turbine model is given in Figure 1(a). The vibration amplitude depends on the magnitude of the wind load f_d as an excitation of the system. The AEMD system is used to suppress the vibration of the system against any f_d wind load. Figure 1(b) shows the schematic view of the active electromagnetic mass damper system. In this structure, there are two identical electromagnets placed opposite to each other on top of the wind turbine nacelle. The electromagnetic force f_a generated by these two electromagnets moves the guided external mass placed between the two electromagnets. The external mass is moved by closed-loop control to suppress the vibration through electromagnetic forces generated by electromagnets.

In this AEMD system model, k_s and c_s represent the stiffness and damping of the nacelle system, respectively. Here, x_s denotes the horizontal movement of the nacelle and

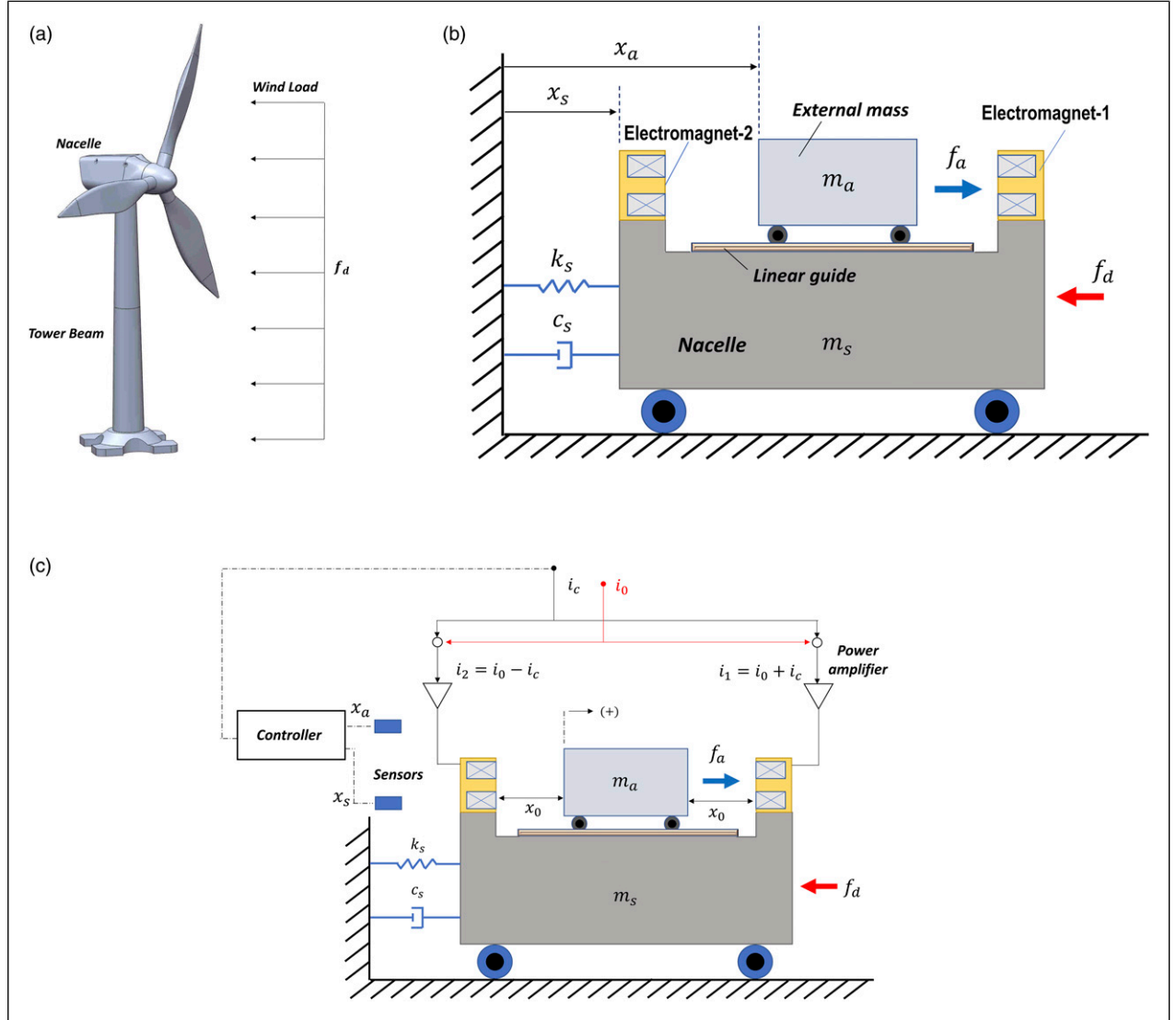


Figure 1. (a) Wind turbine system flow-induced load, (b) active electromagnetic mass damper structure, and (c) schematic representation of the active magnetic system in active electromagnetic mass damper system.

x_a denotes the relative horizontal movement of the stabilizer external mass. Table 1 summarizes the parameter values of the AEMD system. The power parameters of the wind turbine model were selected based on the literature (Martynowicz, 2017). This model was backed up by an additional study of dynamical similarity with a full-scale wind turbine structure.

3. Mathematical model of the system

The motion of the AEMD system consists of two main parts. These are the movement of the nacelle and the movement of the external mass. The dynamic equation of the AEMD system can be written as

$$m_s \ddot{x}_s + c_s \dot{x}_s + k_s x_s = f_d - f_a \quad (1)$$

$$m_a \ddot{\delta}_a = f_a \quad (2)$$

where $\ddot{\delta}_a = \ddot{x}_a - \ddot{x}_s$ shows the absolute acceleration in the system. Also, f_d represents the wind load, which is the exciter of the system, and f_a represents the control force generated by the electromagnets. The power scheme of the electromagnets is shown in Figure 1(c). The system structure is very similar to the axial magnetic bearing structure with a bias current. In this figure, i_0 represents the bias current and i_c represents the active control current. The power amplifiers transmit the required current to the

Table 1. Values of the electromagnetic mass damper system.

Symbol	Meaning	Value	Unit
m_s	Mass of the nacelle system	420	kg
k_s	Stiffness value of the nacelle system	11,200	N/m
c_s	Damping value of the nacelle system	75	Ns/m
m_a	Mass of the ferromagnetic stabilizer	7.35	kg
i_0	Bias current	2.5	A
x_0	Air gap distance	10×10^{-13}	M
μ_0	Magnetic permeability	$4 \times \pi \times 10^{-17}$	H/m
A_c	Coil surface area	5×10^{-13}	m ²
N	Number of turns in coil of the electromagnets	450	—

electromagnets according to the position information. The aerodynamic wind load f_d can be written as

$$f_d = \frac{1}{2} \rho A_s V^2 C_d \quad (3)$$

where ρ is the air density, A_s represents the wind load surface area, V is the wind speed, and finally C_d is the drag coefficient.

The equation of the electromagnetic force (f_e) generated by the pair electromagnets is defined as

$$f_e = f_1 - f_2 = k \left(\frac{(i_0 + i_c)^2}{(x_0 - x_a)^2} - \frac{(i_0 - i_c)^2}{(x_0 + x_a)^2} \right) \quad (4)$$

where f_1 and f_2 are the electromagnetic force generated by the electromagnet pairs and x_0 is the nominal gap between the electromagnet and active mass on both sides as shown in Figure 1(c). The driving of electromagnet 1 and electromagnet 2 in a feedback control structure is realized with the control current i_c . Note that the sensor output x_a of the external mass is set to zero at the initial state (both side gap x_0) in the implementation of this concept. The application of the pair electromagnet is very common in magnetic bearing systems (Maslen and Schweitzer, 2009). Equation (4) is a nonlinear structure and can be linearized as follows

$$f_a = K_x x_a + K_i i_c \quad (5)$$

where K_x represent the force–displacement factor and K_i represents the force–current factor of the electromagnets and i_c is the control current output from the power amplifier. K_x and K_i can be written as follows

$$K_x = 4k \frac{i_0^2}{x_0^3}, \quad K_i = 4k \frac{i_0}{x_0^2} \quad (6)$$

where $k = \mu_0 N^2 A_c / 4$ is the electromagnetic constant.

To ease the presentation of the subsequent backstepping control development, the equation of the motion of the AEMD system can be written as follows

$$m_s \ddot{x}_s + c_s \dot{x}_s + k_s x_s - f_d + K_x x_a = -K_i i_c \quad (7)$$

$$m_a \ddot{x}_a - m_a \ddot{x}_s - K_x x_a = K_i i_c \quad (8)$$

To eliminate \ddot{x}_s term in equation (8), the acceleration \ddot{x}_s is subtracted from equation (7) and substituted in equation (7) which gives

$$m_a \ddot{x}_a + \frac{c_s m_a}{m_s} \dot{x}_s + \frac{k m_a}{m_s} x_s - \frac{f_d m_a}{m_s} + \frac{K_x m_a}{m_s} x_a + \frac{K_i m_a}{m_s} i - K_x x_a = K_i i \quad (9)$$

The dynamic model of the active mass damper system by combining equations (7) and (9) can be arranged in the matrix form

$$\begin{aligned} & \begin{bmatrix} m_s & 0 \\ 0 & m_a \end{bmatrix} \begin{bmatrix} \ddot{x}_s \\ \ddot{x}_a \end{bmatrix} + \begin{bmatrix} c_s & 0 \\ \frac{c_s m_a}{m_s} & 0 \end{bmatrix} \begin{bmatrix} \dot{x}_s \\ \dot{x}_a \end{bmatrix} \\ & + \begin{bmatrix} k_s & K_x \\ \frac{k_s m_a}{m_s} & \frac{K_x m_a}{m_s} - K_x \end{bmatrix} \begin{bmatrix} x_s \\ x_a \end{bmatrix} \\ & + \begin{bmatrix} -1 \\ -\frac{m_a}{m_s} \end{bmatrix} f_d = \begin{bmatrix} -K_i \\ K_i - \frac{K_i m_a}{m_s} \end{bmatrix} i_c \end{aligned} \quad (10)$$

The compact form of the equation is written as

$$[\mathbf{M}][\ddot{\mathbf{q}}] + [\mathbf{C}][\dot{\mathbf{q}}] + [\mathbf{K}][\mathbf{q}] + [\mathbf{F}] f_d = [\mathbf{H}] i_c \quad (11)$$

where $\mathbf{q}^T = [x_s \quad x_a]^T$ is the state vector. Also, $\mathbf{M} \in \mathbb{R}^{2 \times 2}$ is the positive-definite mass matrix, $\mathbf{C} \in \mathbb{R}^{2 \times 2}$ is the damping matrix, $\mathbf{K} \in \mathbb{R}^{2 \times 2}$ is the stiffness matrix, $\mathbf{F} \in \mathbb{R}^{2 \times 2}$ is the force matrix, and finally $\mathbf{H} \in \mathbb{R}^{2 \times 1}$ is the control matrix.

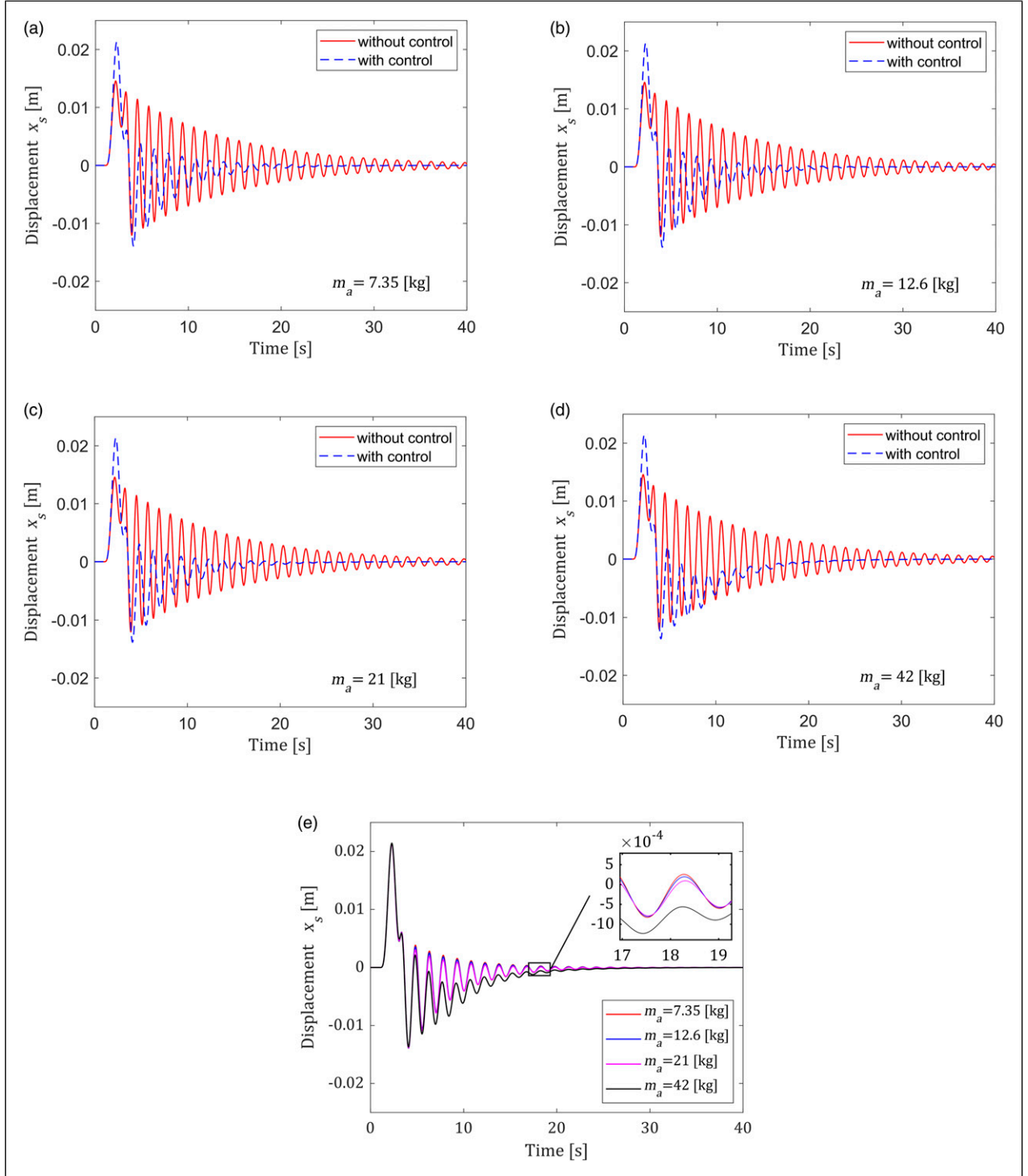


Figure 2. Displacement of the nacelle with and without control for different m_a values: (a) 7.35 kg, (b) 12.6 kg, (c) 21 kg, and (d) 42 kg and (e) comparison for different m_a values.

4. Lyapunov-based adaptive backstepping control

Before starting the controller design, the dynamics of the AEMD system have been converted into the following model class (Fossen, 2002; Fossen and Berge, 1997)

$$\begin{aligned} \dot{\mathbf{q}} &= \mathbf{v} \\ [\mathbf{M}][\dot{\mathbf{v}}] + [\mathbf{C}][\mathbf{v}] + [\mathbf{K}][\mathbf{q}] + [\mathbf{F}]f_d &= [\mathbf{H}]i_c \end{aligned} \quad (12)$$

The position tracking error $\tilde{\mathbf{q}} \in \mathbb{R}^{2 \times 1}$ and its time derivative $\dot{\tilde{\mathbf{v}}} \in \mathbb{R}^{2 \times 1}$ are defined as follows. The goal here is to

find the controller signal that will make $\tilde{q} \rightarrow 0$ as $t \rightarrow \infty$ (Slotine and Li, 1988)

$$\begin{aligned}\tilde{q} &= q - q_d \\ \tilde{v} &= v - v_d\end{aligned}\quad (13)$$

The first step of the backstepping design is defining the virtual control signal

$$\dot{q} = v = s + \alpha \quad (14)$$

where $s = \tilde{v} + \Lambda \tilde{q}$ is the new state vector used for tracking control and α is the stabilizing vector field can be chosen as

$$\alpha = v_r = v_d - \Lambda \tilde{q} \quad (15)$$

where $\Lambda \in \mathbb{R}^{2 \times 2}$ is the positive-definite design matrix of the controller. The combination of (14) and (15) gives

$$v_r = v - s = v_d - \Lambda \tilde{q} \quad (16)$$

To demonstrate the candidate Lyapunov function, the derivative of the position tracking error is written such that

$$\dot{\tilde{q}} = v - v_d = s + \alpha - v_d = -\Lambda \tilde{q} + s \quad (17)$$

Implementation of the backstepping design can be done with the arrangement of the system equations (12) and (16)

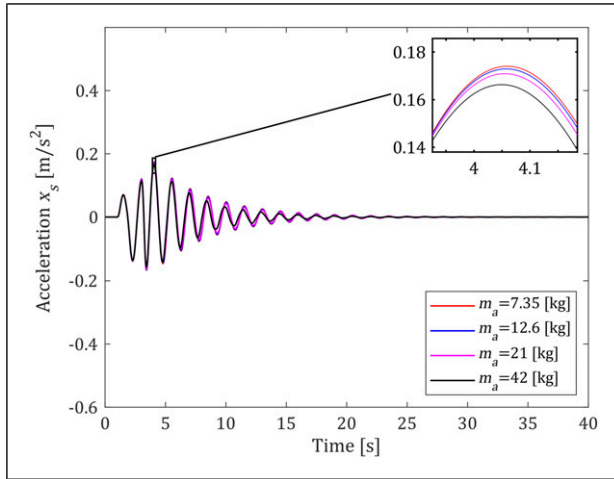


Figure 3. Comparison of the nacelle acceleration for different m_a values.

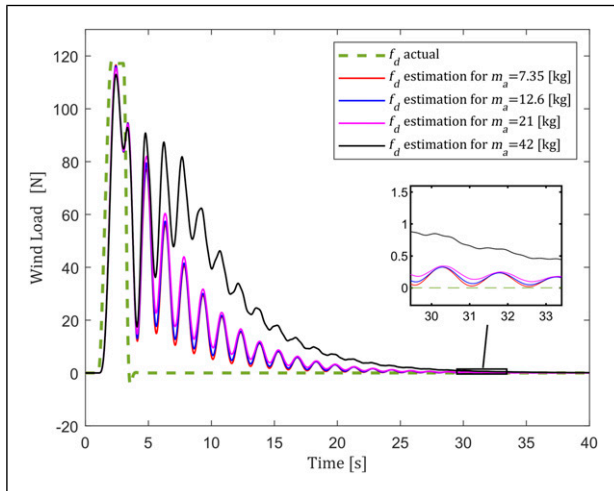


Figure 4. Adaptation of the wind load for different m_a values.

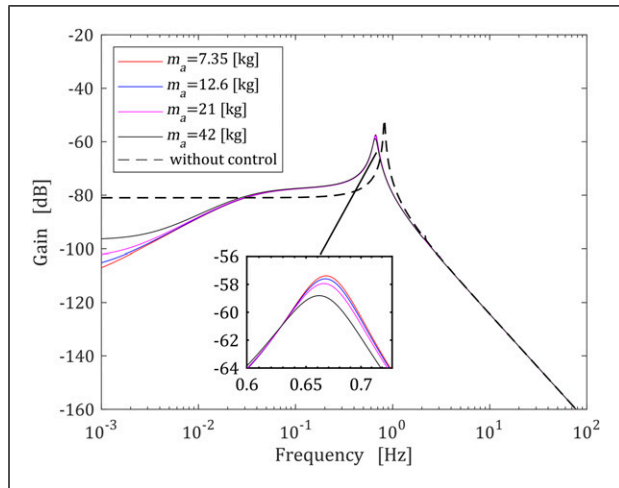


Figure 5. Frequency response of the active electromagnetic mass damper system.

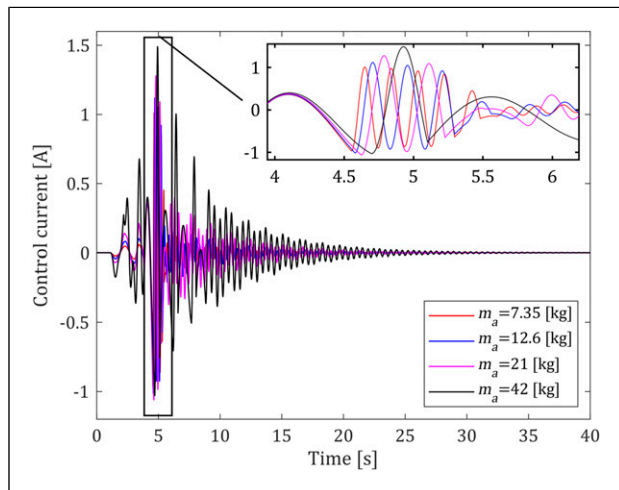


Figure 6. Control currents applied to the electromagnets for different m_a values.

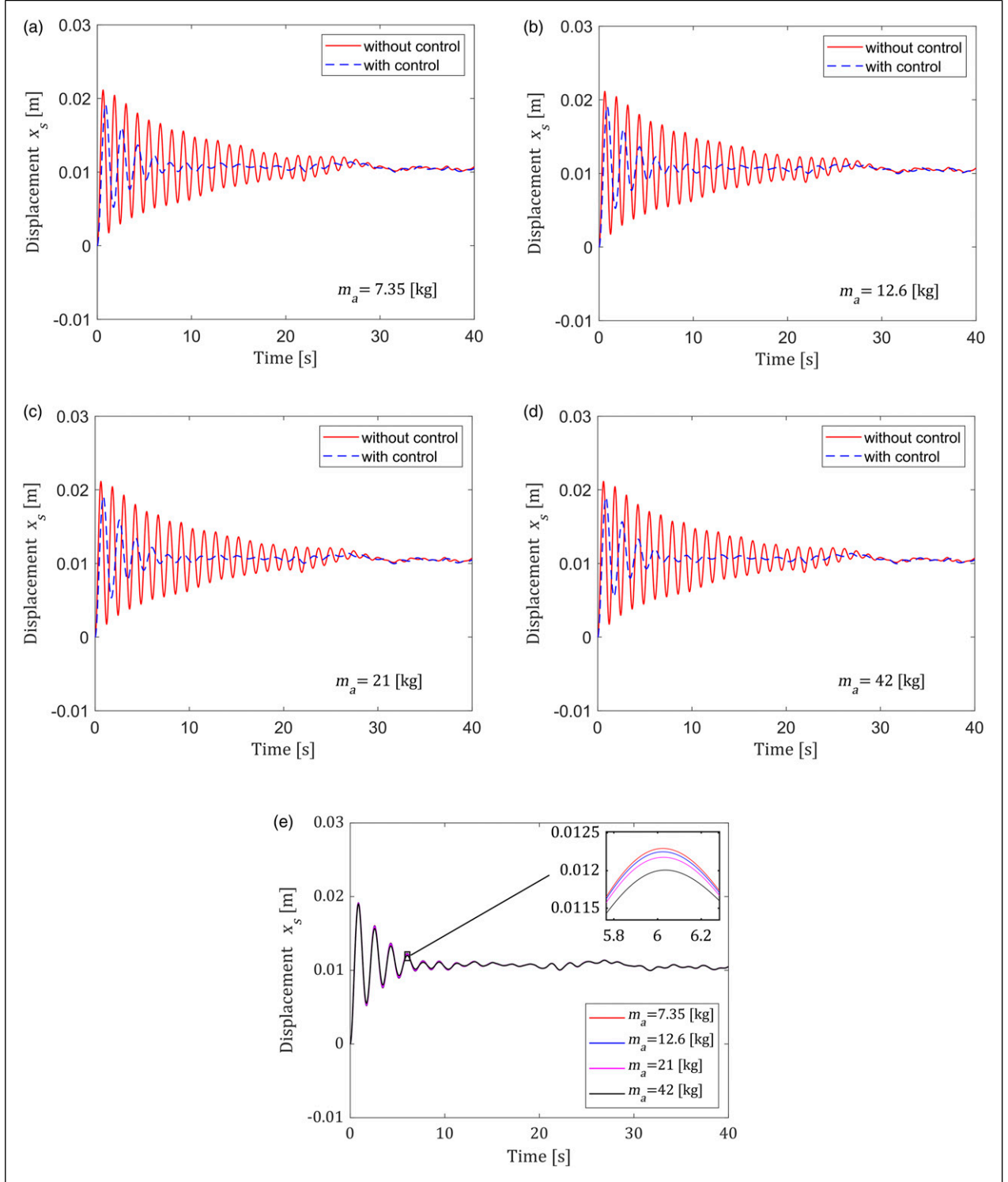


Figure 7. Displacement of the nacelle with and without control for different m_a values under the varying wind load case: (a) 7.35 kg, (b) 12.6 kg, (c) 21 kg, and (d) 42 kg and (e) comparison for different m_a values.

$$\mathbf{M}(\dot{\mathbf{s}} + \dot{\mathbf{v}}_r) + \mathbf{C}(\mathbf{s} + \mathbf{v}_r) + \mathbf{K}\mathbf{q} + \mathbf{F}f_d = \mathbf{H}i_c \quad (18)$$

Arrange the equation as follows

$$\mathbf{M}\dot{\mathbf{s}} + \mathbf{C}\mathbf{s} = \mathbf{H}i_c - \mathbf{M}\dot{\mathbf{v}}_r - \mathbf{C}\mathbf{v}_r - \mathbf{K}\mathbf{q} - \mathbf{F}f_d \quad (19)$$

Here, f_d is the aerodynamic load; it is a constant amplitude parameter calculated based on the constant wind speed. So we cannot eliminate it directly. Now, let us consider \hat{f}_d , which is an estimate of the unknown f_d instead

$$\tilde{f}_d = f_d - \hat{f}_d \quad (20)$$

Consider the Lyapunov candidate function

$$V = \frac{1}{2} \tilde{q}^T \mathbf{K}_p \tilde{q} + \frac{1}{2} s^T \mathbf{M} s + \frac{1}{2\gamma} \tilde{f}_d^2 \quad (21)$$

where $\mathbf{K}_p \in \mathbb{R}^{2 \times 2}$ is the positive-definite design matrix and $\gamma \in \mathbb{R}$ is the positive adaptation gain. Taking the derivative of the Lyapunov function and making arrangement gives

$$\dot{V} = -\tilde{q}^T \mathbf{K}_p \Lambda \tilde{q} + s^T \mathbf{K}_p \tilde{q} + s^T \mathbf{M} \dot{s} + \dot{\tilde{f}}_d \frac{1}{\gamma} \tilde{f}_d \quad (22)$$

With equation (10), the derivative of the Lyapunov function turns into

$$\begin{aligned} \dot{V} = & s^T \left(\mathbf{H} i_c - \mathbf{M} \dot{v}_r - \mathbf{C} v_r - \mathbf{K} q - \mathbf{F} \tilde{f}_d - \dot{\mathbf{F}} \tilde{f}_d - \mathbf{C} s + \mathbf{K}_p \tilde{q} \right) \\ & - \tilde{q}^T \mathbf{K}_p \Lambda \tilde{q} + \dot{\tilde{f}}_d \frac{1}{\gamma} \tilde{f}_d \end{aligned} \quad (23)$$

where $\mathbf{K}_d \in \mathbb{R}^{2 \times 2}$ is the positive-definite design matrix. Because f_d is constant, we can assume that $\dot{\tilde{f}}_d = -\dot{\hat{f}}_d$. The expression $\dot{\hat{f}}_d$ can be selected as follows to make $[s^T \mathbf{F} \tilde{f}_d + \dot{\hat{f}}_d \frac{1}{\gamma} \tilde{f}_d]$ zero in the final state of the derivative expression

$$\dot{\hat{f}}_d = -s^T \mathbf{F} \gamma \quad (24)$$

Control law term can be derived from (22)

$$\mathbf{H} i_c = \mathbf{M} \dot{v}_r + \mathbf{C} v_r + \mathbf{K} q + \mathbf{F} \hat{f}_d - \mathbf{K}_p \tilde{q} - \mathbf{K}_d s \quad (25)$$

Note that the control current i_c obtained by the pseudo-inverse of \mathbf{H} , where

$$\mathbf{H}^\dagger = (\mathbf{H}^T \mathbf{H})^{-1} \mathbf{H}^T \quad (26)$$

If we use the control law signal and the adaptation term in equation (23), then the negative-definite derivative of the Lyapunov function is obtained as

$$\dot{V} = -s^T (\mathbf{C} + \mathbf{K}_d) s - \tilde{q}^T \mathbf{K}_p \Lambda \tilde{q} - s^T \mathbf{F} \tilde{f}_d - \dot{\tilde{f}}_d \frac{1}{\gamma} \tilde{f}_d \quad (27)$$

Because V positive definite and \dot{V} is negative definite, $(\tilde{q}, s) = (0, 0)$ and globally exponential stability is achieved.

5. Simulation study and parametric analysis

In this study, three different assumptions were made for the wind load f_d and simulation studies were conducted. At first, a rectangular pulse of 120 N magnitude wind load input is

assumed to be applied to the wind turbine model. To test the control efficiency under more realistic conditions, a white noise and a sinusoidal wind load inputs were also applied to the system model at the MATLAB Simulink environment, and the control performance was examined under these variable load inputs.

5.1. Constant wind load case

The stabilizer mass (m_a) in the active mass damping systems should be decided in such a way that it does not increase the total mass of the system and at the same time suppresses the vibrations efficiently. In this study, we first chose the stabilizer mass as 7.35 kg, which corresponds to 1.75% of the total system mass. Basically, the total control

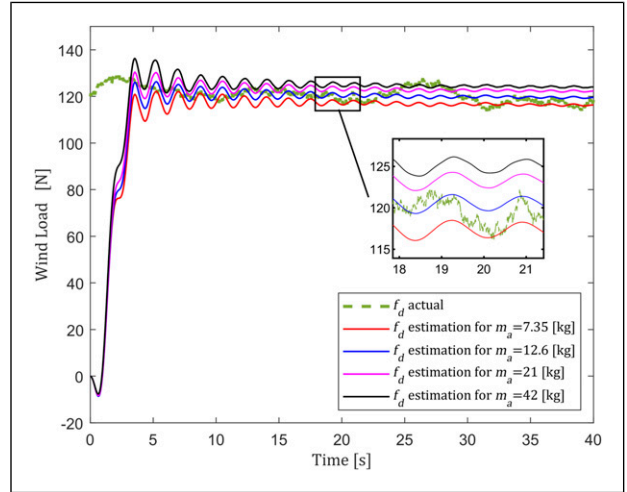


Figure 8. Adaptation of the wind load for different m_a values under the varying wind load case.

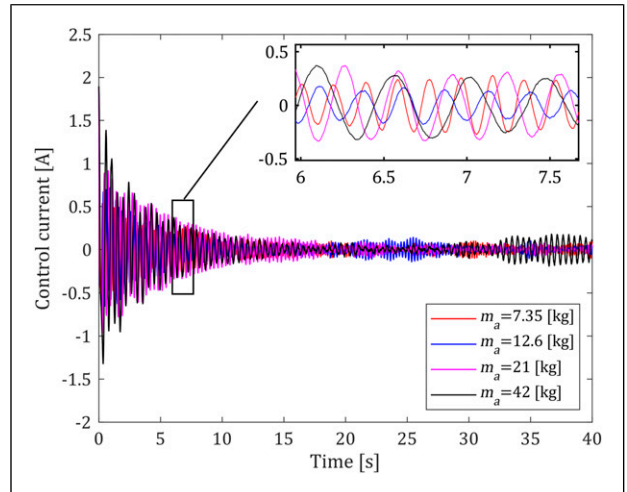


Figure 9. Control currents applied to the electromagnets for different m_a values under the varying wind load case.

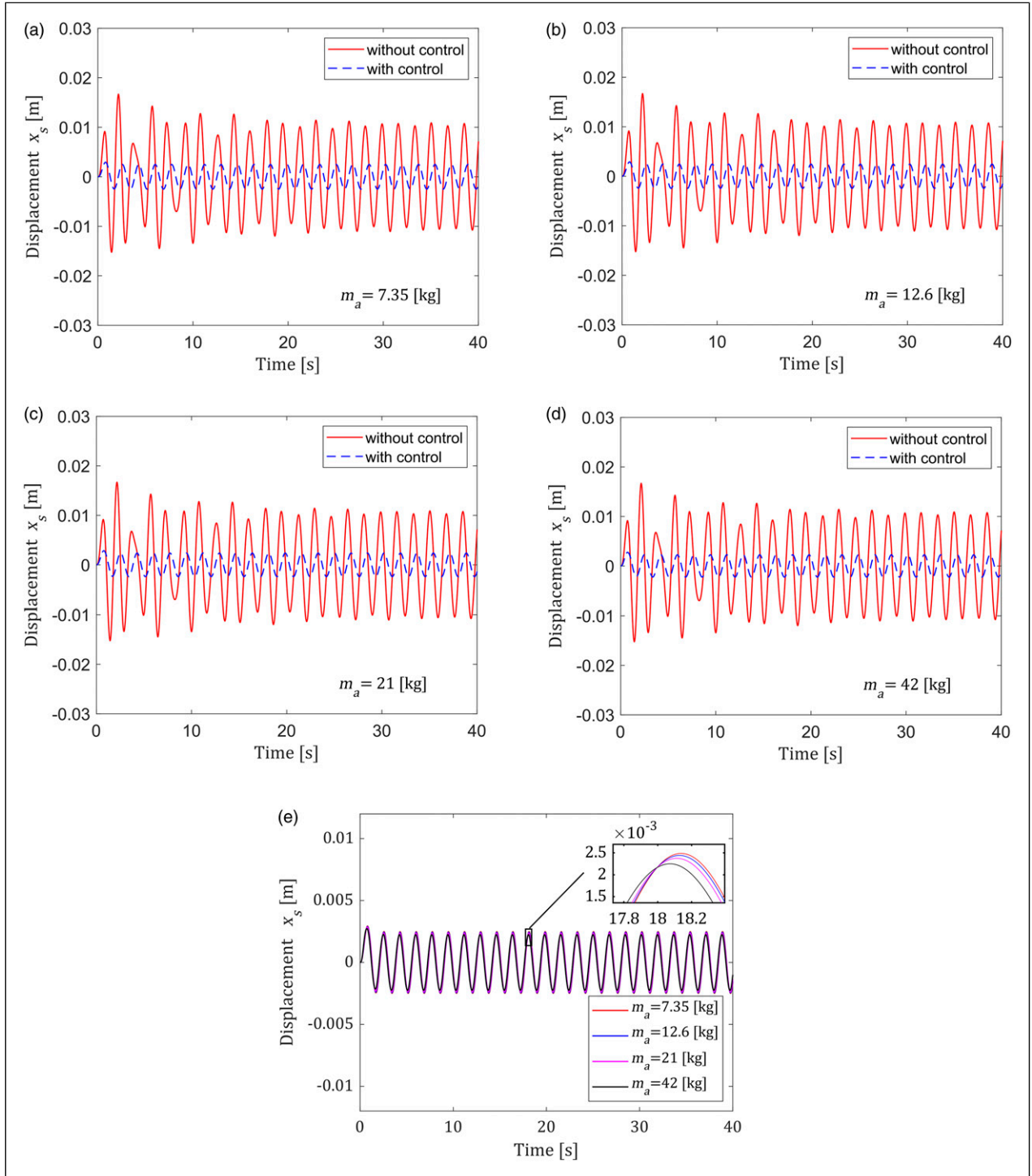


Figure 10. Displacement of the nacelle with and without control for different m_a values under the system frequency-dependent wind load case: (a) 7.35 kg, (b) 12.6 kg, (c) 21 kg, and (d) 42 kg and (e) comparison for different m_a values.

force is directly related to the amount of the stabilizer mass, and selecting such a small value of the stabilizer mass to suppress the vibration is an advantage of the AEMD. For comparison, simulations were repeated for the mass values

of 12.6 kg, 21 kg, and 42 kg, respectively, corresponding to 3%, 5%, and 10% of the total system mass. The designed Lyapunov-type adaptive backstepping controller is tested in the MATLAB Simulink simulation environment for zero

initial condition of the system states. A rectangular-shaped pulse signal (see Figure 4) is used to represent the wind load. Parameters of the designed controller are selected as

$$\begin{aligned} \Lambda &= \begin{bmatrix} 0.9 & \\ & 0.9 \end{bmatrix} \\ \mathbf{K}_p &= \begin{bmatrix} 1 & \\ & 1 \end{bmatrix} \\ \mathbf{K}_d &= \begin{bmatrix} 0.1 & \\ & 0.1 \end{bmatrix} \\ \gamma &= 3700 \end{aligned} \quad (28)$$

To simulate the system behavior under the wind load, the pulse signal wave was applied to the system model between the first and the third seconds. The displacements of the wind turbine nacelle with the pulse load excitation are given in Figure 2. The designed controller effectively suppresses the vibration caused by the wind load. Four different values of m_a are considered in these figures. It is observed that the amplitude of the vibration caused by the wind load on the nacelle has been successfully reduced for all cases. Moreover, Figure 2(e) compares the variation of the nacelle displacement for different values of the stabilizer mass. Similarly, Figure 3 depicts the acceleration results of the wind turbine nacelle under the same load conditions.

The parameter adaptation result is shown in Figure 4. The proposed adaptation approach has the potential to estimate the applied wind load acting on the system. Although the adaptation rate slows as the amount of stabilizer mass increases, it is seen that all values converge to zero over time. To understand the efficiency of the controller, the frequency response of the system is obtained as given in Figure 5. It is observed that the magnitude of the controlled

system frequency response is lower than the uncontrolled system frequency response.

In the active control studies, the magnitude of the control current is a measure of the control performance evaluation. Saturation of the actuator is never desired for real applications. To see the effect of the stabilizer mass on the control currents, the comparison of the currents is given in Figure 6. The obtained control currents are achievable level for the considered electromagnetic actuators. A relation between vibration suppression performance and the amplitude of the control currents can be obtained by comparing Figures 2(e) and 6. When compared with Figure 2e, the increase in the mass of m_a causes the vibration amplitudes to decrease, but it causes an increase in the control currents, and this creates a trade-off problem.

5.2. Varying wind load case

In Section 5.1, the controller was tested under a rectangular pulse wind load condition. In practice, a wind disturbance continuously varies in time with fluctuations due to air turbulence. For a more realistic simulation, the distributed white noise base wind model given in Iov et al. (2004) is applied to the control system model. The wind load profile shown in Figure 8 has an oscillating characteristic around 120 N. The same control parameters given in equation (27) are used in varying wind load simulations. The displacement responses are obtained as shown in Figure 7 when the variable wind load is applied. The controller successfully suppresses the vibration of the nacelle for different m_a values. To understand the effect of different m_a for the varying wind load case, the comparison of the nacelle displacements is also plotted in Figure 7(e).

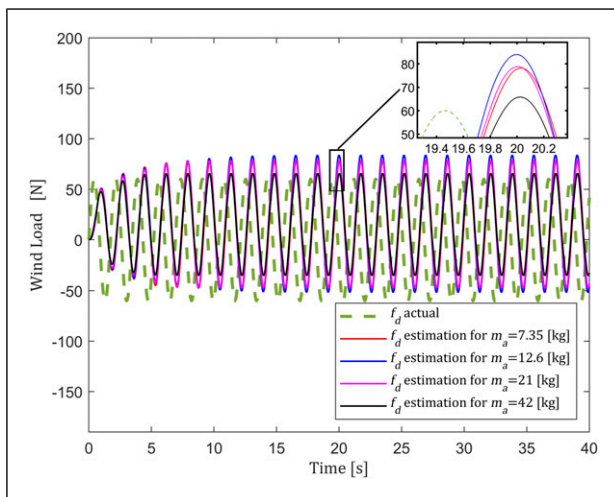


Figure 11. Adaptation of the wind load for different m_a values under the system frequency-dependent wind load.

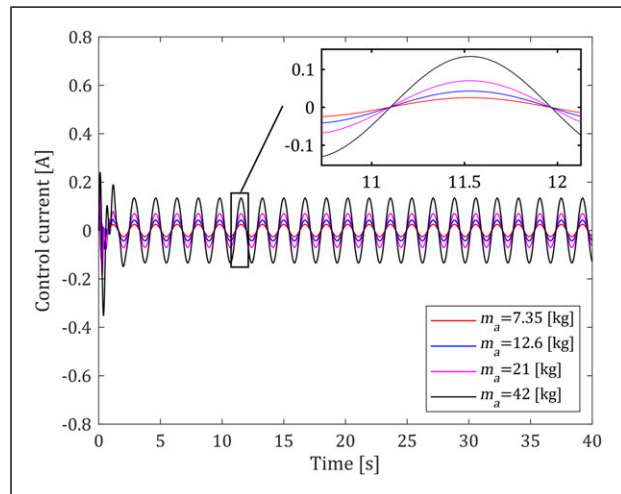


Figure 12. Control currents applied to the electromagnets for different m_a values under the system frequency-dependent wind load.

The parameter adaptation results for the varying wind load case are shown in Figure 8. The tendency in the adaptation of the variable load is on an acceptable level for different active masses. Finally, Figure 9 shows the change in control currents when different masses are used under the varying wind load. The designed controller produces the control current depending on the variation in load condition.

5.3. System frequency-dependent wind load case

In this section, the performance of the designed AEMD system is tested with a steady-state sinusoidal form wind input. Because a sine signal is a frequency-dependent function, it provides a frequency-dependent excitation.

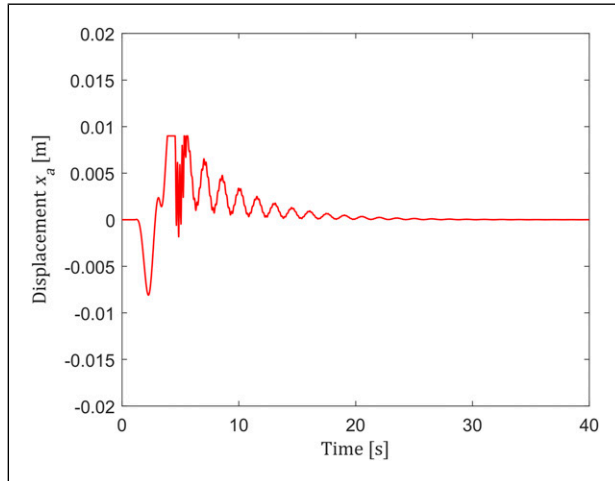


Figure 13. Displacement of the stabilizer mass.

The wind load models defined in the previous sections were independent of the frequency of the system. In this section, system simulations are performed under a wind load with a frequency of 0.578 Hz (see Figure 11). This frequency value corresponds to the first natural frequency of the tower nacelle system after the stabilizer mass has been added. Therefore, the performance of the controller is examined by selecting the natural frequency of the system as the excitation frequency of the wind load. This situation creates a tough condition for the control system model. When wind load with a frequency of 0.578 Hz is applied, the displacement responses for different m_a values are given in Figure 10. Because a steady-state disturbance input affects the system, the displacement amplitude never goes to zero but reduces to a small value by the controller. Moreover, displacements of the nacelle for different active mass values are plotted in Figure 10(e). The parameter adaptation results under the varying wind load case are shown in Figure 11. Finally, Figure 12 shows the change in control currents when different masses are used under the system frequency-dependent wind load case.

6. Verification with electromagnetic finite element analysis

After the simulation study, the amount of the stabilization force, generated by the electromagnets according to the movement of the stabilizer mass for 7.35 kg, was studied using electromagnetic finite element analysis in FEMM package. The horizontal displacement of the stabilizer mass x_a is given in Figure 13. According to the displacement of the stabilizer mass, some points are selected, and the geometry of the finite element model is constructed. In this way, the air gap between the electromagnet and the

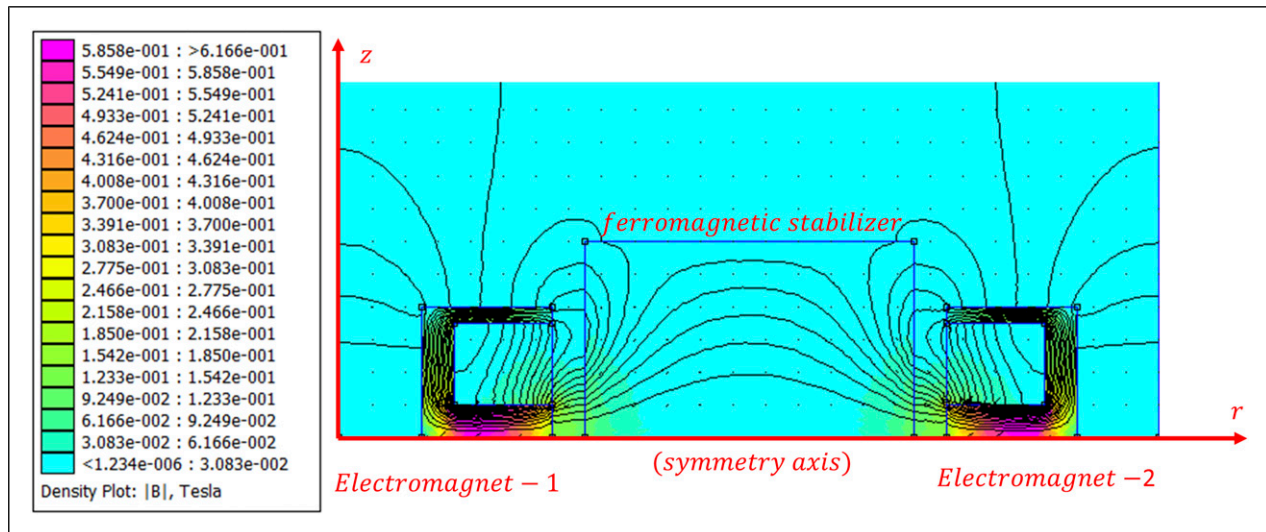


Figure 14. Electromagnetic finite analysis model of the active electromagnetic mass damper system.

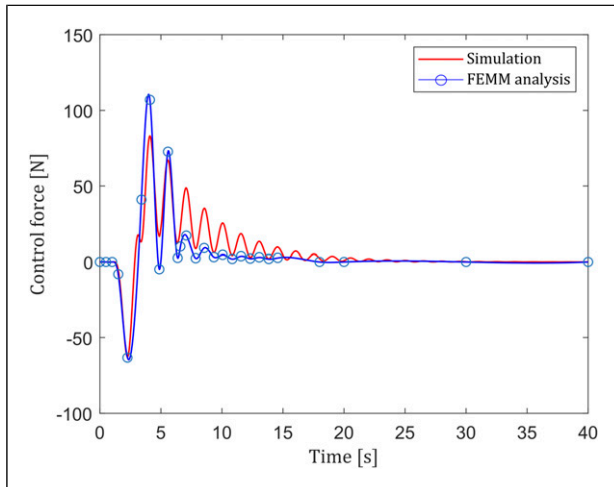


Figure 15. Electromagnetic control force generated by the electromagnets.

ferromagnetic material is adjusted to give the actual magnetic force in every test point. Figure 14 shows the electromagnetic finite analysis model. In this model, the axisymmetric problem is constructed. As seen in the figure, $-r$ axis represents the symmetry axis. The program solves 2D planar and axisymmetric problems in magnetics and electrostatics. The symmetry axis definition is required by the FEMM program. Note that the electromagnets in the figure are seen as a half section. For this reason, the definition of stabilization mass is taken as cylindrical geometry in the program. In terms of magnetic analysis, this acceptance was made as the mass of the ferromagnetic material did not change. Figure 15 compares the electromagnetic control forces generated by the electromagnets obtained from the simulation and finite element analysis. As can be seen, the results are in a good agreement at the start of the simulation. It is observed that finite element results are smaller than simulation results after a certain period. The reason for this situation is because of the saturation in the displacement of the stabilizer mass given in Figure 13. Magnetic force is inherently nonlinear in nature. However, using linear magnetic force expressions in the control design is a frequently applied approach. The difference between simulation results and FEM analysis is because of the unmodeled nonlinearity of the magnetic force. This study will be a good reference that provides a good understanding of the control theory that was done prior to experimental validation.

7. Conclusion

While the wind turbines transform the kinetic energy of the wind into electrical energy through the rotation of blades, they are also exposed to strong vibration in operation due to the wind load. These vibrations can cause damages over time. Active mass dampers have long been known and are

often used to control wind-induced vibrations in high-rise buildings. They are also capable of suppressing wind turbine vibrations. In conventional AMDs, the movement of the active mass is usually provided by servomotors. In this study, a novel-type structure of actuation using electromagnetic actuators is proposed for active mass damper systems. The basic principle used in moving the active mass is to apply the pulling forces created by electromagnets in feedback control. The proposed pair magnet structure with pull-pull electromagnetic forces acting on the mass at any time provides a fast response to any varying load conditions. Therefore, the AEMD system may have the potential to suppress the wind turbine vibration caused by different types of wind load.

In practice, the success of active control also depends on used control methods. The proposed adaptive backstepping control guarantees the stability of the system with the Lyapunov-based approach. In addition, the adaptation property of the proposed control successfully predicts most disturbance load, and this increases the control performance. In simulation studies, vibration suppression of the wind turbine model was successfully achieved under three different load conditions. The obtained results are also promising to the potential application of similar structural systems exposed to wind-induced loads as well as wind turbines.

Finally, a finite element analysis-based verification of the electromagnetic force generated by the electromagnets shows that the designed system is appropriate for vibration suppression in structural systems. The proposed novel AEMD structure can be applicable to small or middle size wind turbine systems. The AEMD concept first needs to be approved with experimental works. For this aim, a laboratory size experimental setup is planned to be established in the future study of this research group.

Declaration of Conflicting Interests

The author(s) declared no potential conflicts of interest with respect to the research, authorship, and/or publication of this article.

Funding

The author(s) received no financial support for the research, authorship, and/or publication of this article.

ORCID iD

Sinan Basaran  <https://orcid.org/0000-0002-3783-2260>

References

- Alkhatib R and Golnaraghi MF (2003) Active structural vibration control: a review. *The Shock and Vibration Digest* 35(5): 367–383. DOI: [10.1177/05831024030355002](https://doi.org/10.1177/05831024030355002).
- Arrigan J, Pakrashi V, Basu B, et al. (2010) Control of flapwise vibrations in wind turbine blades using semi-active tuned mass

- dampers. *Structural Control and Health Monitoring* 18(8): 840–851. DOI: [10.1002/stc.404](https://doi.org/10.1002/stc.404).
- Bathaei A, Zahrai SM and Ramezani M (2018) Semi-active seismic control of an 11-DOF building model with TMD+MR damper using type-1 and -2 fuzzy algorithms. *Journal of Vibration and Control* 24(13): 2938–2953. DOI: [10.1177/1077546317696369](https://doi.org/10.1177/1077546317696369).
- Brodersen ML, Bjørke A-S and Høgsberg J (2016) Active tuned mass damper for damping of offshore wind turbine vibrations. *Wind Energy* 20(5): 783. DOI: [10.1002/we.2063](https://doi.org/10.1002/we.2063).
- Contreras-Lopez J, Ornelas-Tellez F and Espinosa-Juarez E (2019) Optimal control for footbridges' vibration reduction based on semiactive control through magnetorheological dampers. *International Journal of Structural Stability and Dynamics* 19(9): 1950110. DOI: [10.1142/s0219455419501104](https://doi.org/10.1142/s0219455419501104).
- Coppola G and Liu K (2010) Control of a unique active vibration isolator with a phase compensation technique and automatic on/off switching. *Journal of Sound and Vibration* 329(25): 5233–5248. DOI: [10.1016/j.jsv.2010.06.025](https://doi.org/10.1016/j.jsv.2010.06.025).
- Coppola G, Liu K, Liu X, et al. (2013) Experimental study on the control of a novel vibration isolator via adaptive backstepping. *Journal of Vibration and Control* 21(7): 1321–1339. DOI: [10.1177/1077546313497243](https://doi.org/10.1177/1077546313497243).
- Elias S, Matsagar V and Datta TK (2019) Dynamic response control of a wind-excited tall building with distributed multiple tuned mass dampers. *International Journal of Structural Stability and Dynamics* 19(6): 1950059. DOI: [10.1142/s0219455419500597](https://doi.org/10.1142/s0219455419500597).
- Fitzgerald B and Basu B (2013) Active tuned mass damper control of wind turbine nacelle/tower vibrations with damaged foundations. *Key Engineering Materials* 569: 660–667. DOI: [10.4028/www.scientific.net/kem.569-570.660](https://doi.org/10.4028/www.scientific.net/kem.569-570.660).
- Fossen TI (2002) Marine control systems: guidance, navigation and control of ships, rigs and underwater vehicles. Trondheim, Norway. Marine Cybernetics.
- Fossen TI and Berge SP (1997) Nonlinear vectorial backstepping design for global exponential tracking of marine vessels in the presence of actuator dynamics. In: Proceedings of the 36th IEEE Conference on Decision and Control, San Diego, CA, 12 December 1997. Piscataway, NJ: IEEE.
- Hacioglu Y and Yagiz N (2011) Adaptive backstepping control with estimation for the vibration isolation of buildings. *Journal of Vibration and Control* 18(13): 1996–2005. DOI: [10.1177/1077546311429052](https://doi.org/10.1177/1077546311429052).
- Hiramoto K and Grigoriadis KM (2016) Active/semi-active hybrid control for motion and vibration control of mechanical and structural systems. *Journal of Veterinary Cardiology: The Official Journal of the European Society of Veterinary Cardiology* 22(11): 2704–2718. DOI: [10.1177/1077546314550700](https://doi.org/10.1177/1077546314550700).
- Huo L, Song G, Li H, et al. (2007) H_∞ robust control design of active structural vibration suppression using an active mass damper. *Smart Materials and Structures* 17(1): 015021. DOI: [10.1088/0964-1726/17/01/015021](https://doi.org/10.1088/0964-1726/17/01/015021).
- Ikeda Y (2016) An active mass damper designed using ARX models of a building structure. *Earthquake Engineering & Structural Dynamics* 45(13): 2185–2205. DOI: [10.1002/eqe.2754](https://doi.org/10.1002/eqe.2754).
- Iov F, Hansen AD, Sørensen P, et al. (2004) *Wind Turbine Blockset in Matlab/Simulink. General Overview and Description of the Models*. Denmark: Aalborg University. .
- Kwok KCS and Samali B (1995) Performance of tuned mass dampers under wind loads. *Engineering Structures* 17(9): 655–667. DOI: [10.1016/0141-0296\(95\)00035-6](https://doi.org/10.1016/0141-0296(95)00035-6).
- Lackner MA and Rotea MA (2010) Passive structural control of offshore wind turbines. *Wind Energy* 14(3): 373–388. DOI: [10.1002/we.426](https://doi.org/10.1002/we.426).
- Li L and Cui P (2017) Novel design approach of a nonlinear tuned mass damper with duffing stiffness. *Journal of Engineering Mechanics* 143(4): 4017004. DOI: [10.1061/\(asce\)em.1943-7889.0001229](https://doi.org/10.1061/(asce)em.1943-7889.0001229).
- Martynowicz P (2019) Nonlinear optimal-based vibration control for systems with MR tuned vibration absorbers. *Journal of Low Frequency Noise, Vibration and Active Control* 38(3–4): 1607–1628. DOI: [10.1177/1461348418819410](https://doi.org/10.1177/1461348418819410).
- Martynowicz P (2017) Vibration control of wind turbine tower-nacelle model with magnetorheological tuned vibration absorber. *Journal of Vibration and Control* 23(20): 3468–3489. DOI: [10.1177/1077546315591445](https://doi.org/10.1177/1077546315591445).
- Martynowicz P (2016) Study of vibration control using laboratory test rig of wind turbine tower-nacelle system with MR damper based tuned vibration absorber. *Bulletin of the Polish Academy of Sciences Technical Sciences* 64(2): 347–359. DOI: [10.1515/bpasts-2016-0040](https://doi.org/10.1515/bpasts-2016-0040).
- Maslen EH and Schweitzer G (eds) (2009) *Magnetic Bearings*. Berlin Heidelberg: Springer. DOI: [10.1007/978-3-642-00497-1](https://doi.org/10.1007/978-3-642-00497-1).
- Miyata T (2003) Historical view of long-span bridge aerodynamics. *Journal of Wind Engineering and Industrial Aerodynamics* 91(12–15): 1393–1410. DOI: [10.1016/j.jweia.2003.09.033](https://doi.org/10.1016/j.jweia.2003.09.033).
- Ricciardelli F, Pizzimenti AD and Mattei M (2003) Passive and active mass damper control of the response of tall buildings to wind gustiness. *Engineering Structures* 25(9): 1199–1209. DOI: [10.1016/s0141-0296\(03\)00068-3](https://doi.org/10.1016/s0141-0296(03)00068-3).
- Sivrioglu S (2006) Adaptive control of nonlinear zero-bias current magnetic bearing system. *Nonlinear Dynamics* 48(1–2): 175–184. DOI: [10.1007/s11071-006-9081-5](https://doi.org/10.1007/s11071-006-9081-5).
- Sladek JR and Klingner RE (1983) Effect of tuned-mass dampers on seismic response. *Journal of Surgical Education* 109(8): 2004–2009. DOI: [10.1061/\(asce\)0733-9445](https://doi.org/10.1061/(asce)0733-9445).
- Slotine J-JE and Weiping L (1988) Adaptive manipulator control: a case study. *IEEE Transactions on Automatic Control* 33(11): 995–1003. DOI: [10.1109/9.14411](https://doi.org/10.1109/9.14411).
- Soong T and Constantinou M (2014) *Passive and Active Structural Vibration Control in Civil Engineering*. Vienna: Springer Wien.
- Sun C and Jahangiri V (2018) Bi-directional vibration control of offshore wind turbines using a 3D pendulum tuned mass damper. *Mechanical Systems and Signal Processing* 105: 338–360. DOI: [10.1016/j.ymssp.2017.12.011](https://doi.org/10.1016/j.ymssp.2017.12.011).
- Talib E, Shin J-H and Kwak MK (2019) Designing multi-input multi-output modal-space negative acceleration feedback control for vibration suppression of structures using active mass dampers. *Journal of Sound and Vibration* 439: 77. DOI: [10.1016/j.jsv.2018.09.052](https://doi.org/10.1016/j.jsv.2018.09.052).
- Tian L, Rong K, Bi K, et al. (2019) A bidirectional pounding tuned mass damper and its application to transmission tower-line systems under seismic excitations. *International Journal of Structural Stability and Dynamics* 19(6): 1950056. DOI: [10.1142/s0219455419500561](https://doi.org/10.1142/s0219455419500561).
- Wu, Q, Zhao, W, Zhu, W, et al. (2018) A tuned mass damper with nonlinear magnetic force for vibration suppression with wide

frequency range of offshore platform under earthquake loads. *Shock and Vibration* 2018(7): 1–18. DOI: [10.1155/2018/1505061](https://doi.org/10.1155/2018/1505061).

Zhao G, Raze G Paknejad A, et al. (2020) Active nonlinear inerter damper for vibration mitigation of Duffing oscillators. *Journal of Sound and Vibration* 473: 115236. DOI: [10.1016/j.jsv.2020.115236](https://doi.org/10.1016/j.jsv.2020.115236).

Appendix I

Notation

A_c, A_s	electromagnet coil surface area and wind load surface area	K_x, K_i	force–displacement and force–current factors of the electromagnetic actuator
\mathbf{C}	damping matrix of the system equations	k, k_s	electromagnetic constant and stiffness of the nacelle system
C_d	drag coefficient	\mathbf{M}	mass matrix of the system equations
c_s	damping of the nacelle system	m_a, m_s	mass of the ferromagnetic stabilizer and mass of the nacelle
\mathbf{F}	force matrix of the system equations	N	number of turns in the coil of the electromagnets
f_d, f_a	wind load and electromagnetic forces generated by the electromagnet pair	$\mathbf{q}, \mathbf{q}_d, \tilde{\mathbf{q}}$	state variable vector, desired of state variable vector, and position tracking error vector
\hat{f}_d, \tilde{f}_d	estimate of the wind load and estimation error of the wind load	\mathbf{s}	new state vector used for tracking control
\mathbf{H}	control matrix of the system equations	V	wind speed
i_0, i_c	bias current and active control current	$\mathbf{v}, \mathbf{v}_d, \tilde{\mathbf{v}}$	derivative of state variable vector, derivative of desired of state variable vector, and derivative of position tracking error vector
$\mathbf{K}, \mathbf{K}_p, \mathbf{K}_d$	stiffness matrix of the system equations and design matrices of the designed controller	x_0, x_a, x_s	air gap distance of the electromagnet, absolute displacement of the stabilizer external mass, and the nacelle center of mass
		\mathbf{a}	stabilizing vector
		γ	adaptation gain
		δ	relative motion between ferromagnetic stabilizer and mass of the nacelle
		Λ	design matrix of the designed controller
		μ_0	magnetic permeability